J. Plasma Phys. (2025), *vol*. 91, E100
 doi:10.1017/S0022377825100639

Effect of temperature-anisotropic hot protons on proton cyclotron instability in the Earth's outer magnetosphere: a moment-based quasilinear approach

Muhammad Rashid[1], Tahir Aziz[2], Muhammad Sarfraz[1], Muhammad Ahsan Shahzad[3,4], Muhammad Bilal[3,4] and Aman-Ur- Rehman[3,4,5]

[1]Department of Physics, GC University Lahore, Katchery Road, Lahore 54000, Pakistan
[2]Department of Intermediate Studies, GC University Lahore, Katchery Road, Lahore 54000, Pakistan
[3]Department of Physics and Applied Mathematics (DPAM), PIEAS, PO Nilore, Islamabad 44000, Pakistan
[4]Center of Mathematical Sciences (CMS), PIEAS, PO Nilore, Islamabad 44000, Pakistan
[5]Department of Nuclear Engineering (DNE), PIEAS, PO Nilore, Islamabad 44000, Pakistan

Corresponding author: Muhammad Sarfraz, sarfraz_gcu@yahoo.com

(Received 1 February 2025; revision received 14 June 2025; accepted 16 June 2025)

The presence of multi-component protons with their distinct features is confirmed by various space missions in the Earth's outer magnetosphere regions. Isotropic cold protons and anisotropic hot protons significantly influence/modify the dispersion behaviour of various modes and instabilities and regulate the magnetospheric dynamics effectively. Our present study pays attention to the left-hand-polarised proton cyclotron mode, which gets unstable in the large proton temperature anisotropy condition, i.e. $T_{\perp p} > T_{\parallel p}$. Such favourable thermal conditions for protons are extensively observed during the compression of the solar wind against the Earth's magnetic field. To reveal the wave dynamics in more detail, i.e. time-scale variations in the cold and hot proton temperatures and resulting wave-energy density, we further allow the time evolution of our model bi-Maxwellian distribution function in response to the proton cyclotron instability. Based on velocity-moment techniques, we formulated a set of equations comprising an instantaneous dispersion relation, dynamical perpendicular and parallel temperature relations and a wave-energy density equation. For the graphical illustrations of our mathematical results, we choose initial conditions that are relevant to magnetospheric space environments and reported in various experimental studies. Our exact numerical analysis shows the notable impact of hot proton temperature anisotropy and relative density on the real frequency, growth rate, evolution of initial distributions and wave-energy density of the proton cyclotron instability. Such detailed outcomes will be quite helpful for global/local magnetospheric experimental and simulation studies.

Key words: astrophysical plasmas, plasma instabilities, space plasma physics

1. Introduction

In situ observations pervasively indicate the occurrence of non-thermal features, e.g. temperature anisotropy and suprathermal particles in the solar wind and Earth's magnetospheric plasma environments. Such non-thermal characteristics of the initial distribution lead to turbulent enhancements of various waves and instabilities. These enhanced turbulences of electromagnetic fields cover a wide range of lengths and time scales in different dilute space plasmas, e.g. planetary magnetospheric regions. The particles located away from their equilibrium positions get scattered with such amplified fluctuations and relocate themselves in relatively less energetic equilibrium states. Double adiabatic fluid theory seems inadequate to explain such relaxed/bounded states of charge particles observed in various space plasmas (Chew *et al*. 1956). One of the key models appearing to explain such discrepancies between theory and observations is the kinetic formalism on the basis of the linearised Vlasov–Maxwell equations. Extensive studies have successfully established the role of microinstabilities in defining the instability thresholds and states of the particles. For the choice of thermal, geometrical and polarisation limits, various instabilities are quantified using the linearised solution of the Vlasov–Maxwell equations, particle-in-cell simulations and hybrid simulations in the linear and quasilinear regimes of instability evolution/excitation (Feldman *et al*. 1975; Gary *et al*. 1975; Gary & Feldman 1977; Gary *et al*. 1994; Seough & Yoon 2012; Sarfraz 2018; Bilal *et al*. 2023).

The realistic estimations/predictions of various instabilities are the direct consequences of the actual distribution function. Based on the energy and density, electrons are observed in their decomposed forms. Core electrons with relatively high population and low energies are best fitted with the usual standard bi-Maxwellian form. On the other hand, tenuous and energetic halo electrons with extended tails require a power-law distribution, e.g. kappa distribution, for their actual representations (Maksimovic *et al*. 2005; Stverak *et al*. 2008). In fast solar wind conditions, field-aligned *strahl* electrons are usually fitted with a drifting bi-Maxwellian velocity distribution. Focusing on the Earth's magnetospheric space regions, protons are also observed with two distinguishable components based on their density and thermal velocities (Gary *et al*. 1994). Recent observations of the Magnetospheric Multi-scale Mission (MMS) further validate the presence of cold and hot protons with their distinct features (Toledo *et al*. 2021; Liu *et al*. 2024).

Electromagnetic ion cyclotron (EMIC) or proton cyclotron (PC) instability is identified as one of the mechanisms to generate a variety of waves in the solar wind and magnetospheric regions. Amplified fluctuations of nearly PC frequency appear due to PC instability which significantly scatters the energetic protons. In the non-collisional state of space plasmas, PC instability is a major candidate to redefine the perpendicular temperature to gain lower (nearly isotropic) stable states. Proton cyclotron instability has a left-handed polarisation and appears in the large proton perpendicular temperature condition, i.e. $T_{\perp p} > T_{\parallel p}$ (Gary & Winske 1990; Gary 1992). Real oscillatory and imaginary frequency of the proton/ion cyclotron mode is sensitive to the particle and medium structures (Harris 1961; Sagdeev 1961). Previously, notable revisions in the instability threshold conditions were investigated in the presence of different ion compositions, nonlinear effects and field-aligned drifts of different magnitudes (Maruca 2012; Matteini 2012; Isenberg 2013). In the solar wind conditions, Shaaban *et al*. (2016) revealed the impact of the interplay between anisotropic core–halo protons and non-thermal parameter of halo protons on the dispersion properties and resulting threshold conditions of EMIC instability.

https://doi.org/10.1017/S0022377825100639 Published online by Cambridge University Press

In the empirical relation $T_{\perp i}/T_{\parallel i} = 1 + S\beta_{\parallel i}^{-\alpha}$ of the marginal stability condition of EMIC (or PC) instability, the dimensionless parameters (S, α) have been reported in a hybrid simulation (Gary *et al*. 1994), observation fitting method (Anderson 1996) and with the solution of the linearised Vlasov equation (Gary *et al*. 1994). From the observational perspective, Gary *et al*. (1994) and Toledo *et al*. (2021) reported the presence of multi-proton components in the Earth's magnetosphere. Based on these notable achievements, the dispersion characteristics of strictly parallel PC (Gary *et al*. 1994) and oblique EMIC (Toledo *et al*. 2021) are studied for the conditions typical of magnetospheric regions.

In the recent past, quasilinear analysis appeared as a robust mathematical tool to study and re-examine wave dynamics in more detail. Based on such a simplified nonlinear or reduced quasilinear approach, we can trace the back actions of various unstable modes on the particle distributions. Such comprehensive and more physics-based techniques are quite helpful to display the time variation in physical quantities which otherwise are observed in experimental (Vinas *et al*. 2010) or simulation (Hellinger 2014; Sarfraz *et al*. 2022) studies. Guided by observational magnetospheric data (Gary *et al*. 1994; Toledo *et al*. 2021; Liu *et al*. 2024), we take cold protons as thermally isotropic and adopt anisotropic hot protons as being distributed in a bi-Maxwellian manner. For our choice of different initial outer magnetospheric conditions, we will solve exactly numerically the set of instantaneous dispersion relation, dynamical temperature equations and wave-energy density equation. We will make use of a FORTRAN compiler to build and execute our required files and plot them in Matlab. The quasilinear evolution technique for the proton/ion cyclotron instability was applied in the case of single bi-Maxwellian-distributed ions (Seough & Yoon 2012) and the results were also validated/confirmed in simulations (Seough *et al*. 2014). Later on, Shaaban *et al*. (2021) extended these findings for non-thermal kappa-distributed ions in solar wind conditions. To our best knowledge, there has not yet been an investigation of the isotropic cold and anisotropic hot proton components in magnetospheric conditions. For the case of electrons, Sarfraz *et al*. (2016) have successfully demonstrated the time variations/saturations in the core and halo distributions and the resulting wave intensity. With the help of the quasilinear evolution technique, they were also able to define the marginal stability curves in phase space which otherwise are deduced through simulation or observational fitting method (Lazar *et al*. 2015). Some important quasilinear studies for ions (Yoon & Seough 2012; Yoon *et al*. 2012; Seough *et al*. 2013), electrons (Sarfraz *et al*. 2017; Sarfraz 2018) and the combination there of (Shaaban *et al*. 2019; Sarfraz & Yoon 2019) and validation against simulations (Seough *et al*. 2014; Kim 2017) motivate us to adopt this technique to report the dynamics of PC instability in the Earth's magnetospheric region.

The plan of this paper is as follows. Section 2 describes the mathematical background and the model distribution for the quasilinear evolution of PC instability. Section 3 presents the numerical solutions of self-consistent quasilinear kinetic equations for the different input set-up formed with anisotropic hot protons and their relative density. The conclusion is presented in § 4.

2. Mathematical background

We assume a homogeneous, poorly collisional and non-relativistic magnetospheric electron–proton plasma. Protons are further decomposed into their cold and hot components (Gary *et al*. 1994; Toledo *et al*. 2021; Liu *et al*. 2024). In the aforementioned conditions, the PC frequency, ω, and wave vector, k (propagating strictly

https://doi.org/10.1017/S0022377825100639 Published online by Cambridge University Press

along the ambient magnetic field), satisfy the following instantaneous dispersion relation (Gary 1993; Schlickeiser 2002):

$$\frac{c^2k^2}{\omega^2} = 1 + \sum_{\sigma=e,c,h} \frac{\omega_{p\sigma}^2}{\omega^2} \int \mathrm{d}\boldsymbol{v}\, \frac{v_\perp/2}{\omega - kv_\parallel \pm \Omega_\sigma} \times \left((\omega - kv_\parallel) \frac{\partial f_\sigma}{\partial v_\perp} + kv_\perp \frac{\partial f_\sigma}{\partial v_\parallel} \right), \tag{2.1}$$

where $\sigma = e, c, h$ represents electrons and cold/hot proton components. We use '+' and '−' to differentiate between right- and left-hand polarisations, respectively; $\omega_{p\sigma} = (4\pi n_0 e^2/m_\sigma)^{1/2}$ represents the plasma frequency; e, c, n_0 and m_σ designate the unit electric charge, speed of light in vacuum, total number density and mass of protons species labelled σ, respectively; $\Omega_\sigma = eB_0/m_\sigma c$ is the PC frequency, where B_0 represents the intensity of the ambient magnetic field.

To re-examine the wave dynamics in more detail and possible back action of the PC instability on the initial cold and hot proton distributions, we will make use of reduced macroscopic quasilinear theory. A moment-based quasilinear theory makes use of the following particle kinetic equation under the diffusion approximation:

$$\frac{\partial f_\sigma}{\partial t} = \frac{ie^2}{4m_\sigma^2 c^2} \frac{1}{v_\perp} \int_{-\infty}^{\infty} \frac{\mathrm{d}k}{k^2} \left[\left(\omega^* - kv_\parallel\right) \frac{\partial}{\partial v_\perp} + kv_\perp \frac{\partial}{\partial v_\parallel} \right] \times \frac{v_\perp \delta B^2(k,\omega)}{\omega - kv_\parallel \pm \Omega_\sigma} \left[\left(\omega - kv_\parallel\right) \frac{\partial f_\sigma}{\partial v_\perp} + kv_\perp \frac{\partial f_\sigma}{\partial v_\parallel} \right], \tag{2.2}$$

where $\omega = \omega_k + \mathrm{i}\gamma_k$ represents the complex root of (2.1). Results of (2.1) in the form of real oscillatory frequency ω_r and growth rate γ_k will affect the nonlinear evolution of PC instability. Here, $\delta B^2(k)$ is the spectral wave energy density associated with PC magnetic field perturbations.

2.1. *Model distribution function*

In situ measurements recorded during various space missions located in magnetospheric regions guide us to take the protons in their constituent components. We adopt the following bi-Maxwellian form of the velocity distribution:

$$f_\sigma = \frac{1}{\pi^{3/2}\alpha_{\perp\sigma}^2(t)\alpha_{\parallel\sigma}(t)} \exp\left(-\frac{v_\perp^2}{\alpha_{\perp\sigma}^2(t)} - \frac{v_\parallel^2}{\alpha_{\parallel\sigma}^2(t)} \right) \tag{2.3}$$

all the time, except that we allow the perpendicular and parallel temperatures to vary in time t. Here $\sigma = e, c, h$ stands for electrons and cold/hot protons. For the linear stability analysis of the PC mode, we will adopt cold protons as thermally isotropic and hot protons as anisotropic. As the instability will enter the nonlinear phase, the time variations in the cold/hot proton temperatures will be helpful to examine the loss or gain in the initial anisotropy values. In (2.3), $\alpha_{\perp\sigma}$ and $\alpha_{\parallel\sigma}$ stand for perpendicular and parallel thermal speeds for each species labelled σ, which are defined by

$$T_{\perp\sigma} = \frac{m_\sigma}{2} \int \mathrm{d}\boldsymbol{v} v_\perp^2 f_\sigma = \frac{m_\sigma \alpha_{\perp\sigma}^2}{2},$$
$$T_{\parallel\sigma} = m_\sigma \int \mathrm{d}\boldsymbol{v} v_\parallel^2 f_\sigma = \frac{m_\sigma \alpha_{\parallel\sigma}^2}{2}, \tag{2.4}$$

https://doi.org/10.1017/S0022377825100639 Published online by Cambridge University Press

and m_σ is the mass of charged species labelled σ. The perpendicular and parallel velocity vector components are defined by $v_\perp$ and $v_\parallel$ in cylindrical coordinates. We have omitted the Boltzmann constant, such that the thermal energy is in c.g.s. energy units.

Our approximation of allowing the time variation in thermal velocities, $\alpha_{\perp\sigma}(t)$ and $\alpha_{\perp\sigma}(t)$, may lead to a notable distortion in the distribution (Hellinger 2014) in response to the excitation of PC instability in the nonlinear phase. From the various simulation studies conducted to see the evolution of the distribution function (Seough *et al*. 2014; Kim 2017), it is noted that any change in the initial distribution will only be in the transit states. In the later time of the instability evolution, particles with initial high perpendicular velocities start to diffuse along the pitch angle paths. A nearly isotropic form of the distribution is recovered at the end of the simulation run, which largely validates our assumption regarding the form of the velocity distribution. Such an assumption has been successfully tested in various comparative quasilinear versus simulation studies (Seough *et al*. 2014, 2015; Yoon *et al*. 2015, 2017; Sarfraz *et al*. 2022) and displayed more than good agreement between results. These better comparative findings for the different instabilities motivate us to adopt this approximation and allow us to re-examine the wave dynamics more carefully and in detail.

Under the application of our model function distribution given in (2.3), the complex frequency and wavenumber satisfy the following equation:

$$0 = \frac{c^2k^2}{\omega^2} - \sum_{\sigma=e,c,h} \frac{\omega_{p\sigma}^2}{\omega^2}\left\{\frac{T_{\perp\sigma}}{T_{\parallel\sigma}} - 1 + \left[\frac{T_{\perp\sigma}}{T_{\parallel\sigma}}\,\omega \pm \left(\frac{T_{\perp\sigma}}{T_{\parallel\sigma}} - 1\right)\Omega_\sigma\right]\frac{1}{k\alpha_{\parallel\sigma}}\,Z\left(\frac{\omega \pm \Omega_\sigma}{k\alpha_{\parallel\sigma}}\right)\right\}. \quad (2.5)$$

In (2.5) the plasma dispersion function is defined by $Z(\zeta) = \int_{-\infty}^{\infty}(x-\zeta)^{-1}e^{-x^2}\,\mathrm{d}x$. In the mathematical procedure to reach the instantaneous dispersion relation (2.5), we have ignored the displacement current, as we are not interested in fast waves, i.e. we assume $ck/\omega \gg 1$ here. For the left-hand circularly polarised mode, we may take electrons as isotropic ($T_{\perp e} = T_{\parallel e} = T_e$) and ignore their thermal effects, i.e $\omega \mp |\Omega_e|/k\alpha_{\parallel e} \gg 1$. We approximate $\omega - \Omega_e \approx |\Omega_e|$ and make use of $\omega_{pe}^2/\omega^2(\mp|\Omega_e|) = \omega_{pp}^2/\omega^2(\mp\Omega_p)$ to get the final dispersion relation of the PC mode as

$$\begin{aligned} 0 = {} & \frac{c^2k^2}{\omega_p^2} + \frac{\omega}{\Omega_p} \\ & - \frac{n_c}{n_0}\left\{\frac{T_{\perp c}}{T_{\parallel c}} - 1 + \left[\frac{T_{\perp c}}{T_{\parallel c}}\,\omega - \left(\frac{T_{\perp c}}{T_{\parallel c}} - 1\right)\Omega_p\right]\frac{1}{k\alpha_{\parallel c}}\,Z\left(\frac{\omega - \Omega_p}{k\alpha_{\parallel c}}\right)\right\} \\ & - \frac{n_h}{n_0}\left\{\frac{T_{\perp h}}{T_{\parallel h}} - 1 + \left[\frac{T_{\perp h}}{T_{\parallel h}}\,\omega - \left(\frac{T_{\perp h}}{T_{\parallel h}} - 1\right)\Omega_e\right]\frac{1}{k\alpha_{\parallel h}}\,Z\left(\frac{\omega - \Omega_p}{k\alpha_{\parallel h}}\right)\right\}. \end{aligned} \quad (2.6)$$

Taking the velocity moments for the model distribution function (2.3), the particle kinetic equation (2.2) for the left-hand-polarised mode can be rewritten in the form

https://doi.org/10.1017/S0022377825100639 Published online by Cambridge University Press

of dynamic temperatures as

$$\frac{\mathrm{d}T_{\perp c}}{\mathrm{d}t} = -\frac{e^2}{2m_p c^2}\int_{-\infty}^{\infty}\frac{\mathrm{d}k}{k^2}\,\delta B^2(k)\left\{\left(\frac{2T_{\perp c}}{T_{\parallel c}}-1\right)\gamma_k + \mathrm{Im}\,\frac{2i\gamma_k-\Omega_p}{k\alpha_{\parallel c}}\left[\frac{T_{\perp c}}{T_{\parallel c}}\,\omega-\left(\frac{T_{\perp c}}{T_{\parallel c}}-1\right)\Omega_p\right]\times Z\left(\frac{\omega-\Omega_p}{k\alpha_{\parallel c}}\right)\right\},$$

$$\frac{\mathrm{d}T_{\parallel c}}{\mathrm{d}t} = \frac{e^2}{m_p c^2}\int_{-\infty}^{\infty}\frac{\mathrm{d}k}{k^2}\,\delta B^2(k)\left\{\frac{T_{\perp c}}{T_{\parallel c}}\,\gamma_k + \mathrm{Im}\,\frac{\omega-\Omega_p}{k\alpha_{\parallel\sigma}}\left[\frac{T_{\perp c}}{T_{\parallel c}}\,\omega-\left(\frac{T_{\perp c}}{T_{\parallel c}}-1\right)\Omega_p\right]\times Z\left(\frac{\omega-\Omega_p}{k\alpha_{\parallel c}}\right)\right\},$$

$$\frac{\mathrm{d}T_{\perp h}}{\mathrm{d}t} = -\frac{e^2}{2m_p c^2}\int_{-\infty}^{\infty}\frac{\mathrm{d}k}{k^2}\,\delta B^2(k)\left\{\left(\frac{2T_{\perp h}}{T_{\parallel h}}-1\right)\gamma_k + \mathrm{Im}\,\frac{2i\gamma_k-\Omega_p}{k\alpha_{\parallel h}}\left[\frac{T_{\perp h}}{T_{\parallel h}}\,\omega-\left(\frac{T_{\perp h}}{T_{\parallel h}}-1\right)\Omega_p\right]\times Z\left(\frac{\omega-\Omega_p}{k\alpha_{\parallel h}}\right)\right\},$$

$$\frac{\mathrm{d}T_{\parallel h}}{\mathrm{d}t} = \frac{e^2}{m_p c^2}\int_{-\infty}^{\infty}\frac{\mathrm{d}k}{k^2}\,\delta B^2(k)\left\{\frac{T_{\perp h}}{T_{\parallel h}}\,\gamma_k + \mathrm{Im}\,\frac{\omega-\Omega_p}{k\alpha_{\parallel h}}\left[\frac{T_{\perp h}}{T_{\parallel h}}\,\omega-\left(\frac{T_{\perp h}}{T_{\parallel h}}-1\right)\Omega_p\right]\times Z\left(\frac{\omega-\Omega_p}{k\alpha_{\parallel h}}\right)\right\}. \tag{2.7}$$

The wave kinetic equation is given by

$$\frac{\partial\delta B^2(k)}{\partial t} = 2\gamma_k\,\delta B^2(k). \tag{2.8}$$

In deriving the set of self-consistent quasilinear kinetic (2.6), (2.7) and (2.8), we also assume a homogeneous plasma and wave propagation is strictly parallel (or antiparallel) to the ambient field. Introducing the obliqueness in the propagation will change the threshold conditions and may result in the excitation of the mirror instability (Yoon *et al*. 2012, 2022) in the multi-component proton plasma. This is of course our future task and is beyond the scope of our present study.

3. Numerical analysis

To achieve the exact numerical analysis of (2.6), (2.7) and (2.8), we normalise them with following dimensionless quantities:

https://doi.org/10.1017/S0022377825100639 Published online by Cambridge University Press

$$\zeta_c = \frac{z-1}{q\beta_c^{1/2}}, \qquad \zeta_h = \frac{z-1}{q\beta_h^{1/2}},$$
$$A_c = \frac{\beta_{\perp c}}{\beta_{\parallel c}} - 1, \qquad A_h = \frac{\beta_{\perp h}}{\beta_{\parallel h}} - 1,$$
$$z = \frac{\omega}{\Omega_p}, \qquad q = \frac{ck}{\omega_p}, \qquad \delta = \frac{n_h}{n_0},$$
$$\beta_c = \frac{8\pi n_c T_{\parallel c}}{B_0^2}, \qquad \beta_h = \frac{8\pi n_h T_{\parallel h}}{B_0^2},$$
$$\eta_c = \frac{(A_c+1)z - A_c}{q\beta_{\parallel c}^{1/2}}, \qquad \eta_h = \frac{(A_h+1)z - A_h}{q\beta_{\parallel h}^{1/2}},$$
$$\tau = \Omega_p t, \qquad W(q) = \frac{\delta B^2(q)}{B_0^2}. \tag{3.1}$$

Importantly, the plasma beta definitions of cold and hot protons, $\beta_{\parallel c}$ and $\beta_{\parallel h}$, are consistent with those adopted by Lazar *et al*. (2018) and Yoon *et al*. (2024) for core–halo electron components. With these normalised quantities, the instantaneous dispersion relation (2.6), dynamical perpendicular and parallel temperatures of the constituent proton components (2.7) and the wave-energy density form (2.8) are rewritten as

$$0 = q^2 + z - (1-\delta)\left[A_c + \eta_c Z(\zeta_c)\right] - \delta\left[A_h + \eta_h Z(\zeta_h)\right], \tag{3.2}$$

$$\frac{\mathrm{d}\beta_{\perp c}}{\mathrm{d}\tau} = -2\int_0^\infty \mathrm{d}q\, \frac{W(q)}{q^2}\left[(2A_c+1)\, z_i + \mathrm{Im}\,(2iz_i - 1)\,\eta_c Z(\zeta_c)\right],$$
$$\frac{\mathrm{d}\beta_{\parallel c}}{\mathrm{d}\tau} = 4\int_0^\infty \mathrm{d}q\, \frac{W(q)}{q^2}\left[(A_c+1)\, z_i + \mathrm{Im}\,(z-1)\,\eta_c Z(\zeta_c)\right],$$
$$\frac{\mathrm{d}\beta_{\perp h}}{\mathrm{d}\tau} = -2\int_0^\infty \mathrm{d}q\, \frac{W(q)}{q^2}\left[(2A_h+1)\, z_i + \mathrm{Im}\,(2iz_i - 1)\,\eta_h Z(\zeta_h)\right],$$
$$\frac{\mathrm{d}\beta_{\parallel h}}{\mathrm{d}\tau} = 4\int_0^\infty \mathrm{d}q\, \frac{W(q)}{q^2}\left[(A_h+1)\, z_i + \mathrm{Im}\,(z-1)\,\eta_h Z(\zeta_h)\right], \tag{3.3}$$

$$\frac{\partial W(q)}{\partial \tau} = 2z_i W(q). \tag{3.4}$$

The above set of equations are now implicit functions of five input variables, i.e. δ, β_c, β_h, A_c and A_h. To solve them exactly numerically, we develop codes for the linear and quasilinear evolution of PC instability in Absoft Fortran to generate the required files based on different sets of initial conditions. We then formulate

https://doi.org/10.1017/S0022377825100639 Published online by Cambridge University Press

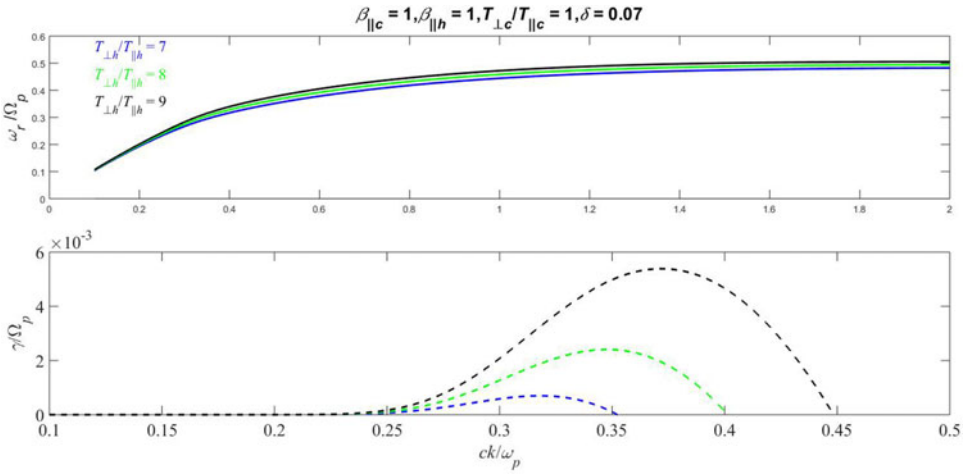

FIGURE 1. Effect of hot proton anisotropy on the dispersion properties of the PC mode: real oscillatory frequency, ω_r/Ω_p (top; solid), and growth rate, γ_k/Ω_p (bottom; dashed), versus normalised wavenumber, ck/ω_p, for different combinations of temperature ratio of hot protons.

programs in Matlab to sketch graphically these executed files. Our choice of initial conditions to run the codes is typical of the magnetospheric conditions suggested in Gary *et al*. (1994), Toledo *et al*. (2021) and Liu *et al*. (2024). To start with, figure 1 is plotted with the following conditions:

$$\frac{T_{\perp c}(0)}{T_{\|c}(0)} = \frac{\beta_{\perp c}(0)}{\beta_{\|c}(0)} = 1,$$
$$\frac{T_{\perp h}(0)}{T_{\|h}(0)} = \frac{\beta_{\perp h}(0)}{\beta_{\|h}(0)} = 7,\ 8,\ 9,$$
$$\beta_{\|c}(0) = 1, \quad \beta_{\|h}(0) = 1, \quad \delta = 0.07. \tag{3.5}$$

The details of these parameters are also provided in the figure title and within the plot. We display the impact of the anisotropic hot proton component on the real oscillatory wave frequency, ω_r, in the top panel and growth rate, γ_k, shown in the bottom panel against the propagation vector, k. As given in (3.1), we normalise the real frequency with the PC frequency, i.e. ω_r/Ω_p, and wave vector with proton skin depth, i.e. ck/Ω_p, and plot them on the x axis and y axis, respectively. We also differentiate the real and imaginary parts of the wave frequency with solid (upper) and dashed (lower) curves, respectively. Based on the average values of observed parameters given in Gary *et al*. (1994) and Toledo *et al*. (2021), we choose a range of hot proton perpendicular temperature anisotropy, i.e. $T_{\perp h}/T_{\|h} = 7{-}9$, and keep the cold protons as thermally isotropic, i.e. $T_{\perp c}/T_{\|c} = 1$. Furthermore, we adopt the range of hot proton relative density, δ, using the geosynchronous orbit set (Gary *et al*. 1994, 1995; Toledo *et al*. 2021) and EMIC mirror mode activities observed by MMS-1 (Toledo *et al*. 2021; Liu *et al*. 2024). Observations of these individual data set points correspond to the data (i) 11–20 November 1994 and (ii) 21–31 January 1994. We keep the initial relative hot proton density and plasma betas of both proton components as fixed. Shown in figure 1, initial higher perpendicular anisotropy supports the real oscillatory frequency of the PC mode (solid black curve).

https://doi.org/10.1017/S0022377825100639 Published online by Cambridge University Press

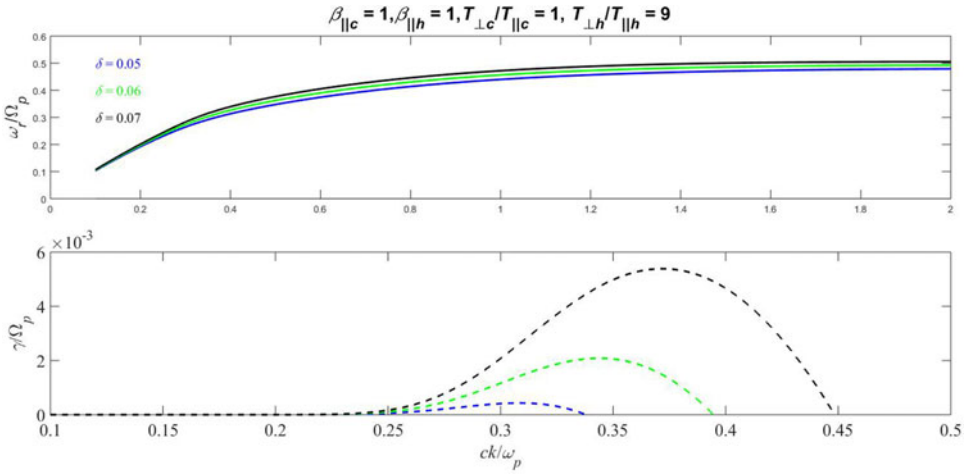

FIGURE 2. Effect of hot proton population on the dispersion properties of the PC mode: real oscillatory frequency, ω_r/Ω_p (top; solid), and growth rate, γ_k/Ω_p (bottom; dashed), versus normalised wavenumber, ck/ω_p, for different combinations of hot proton relative density values.

Similarly, the growth rate of PC instability keeps rising with the higher anisotropy ratio of the hot proton component (see the dashed black curve). A significant rise in the imaginary frequency (growth rate) of the PC wave validates the presence of more free energy associated with hot proton perpendicular temperature anisotropy.

The impact of hot proton relative density in modifying/altering the dispersion characteristics of the PC mode is shown in figure 2. We make a choice of the following initial conditions:

$$\begin{aligned} \delta &= 0.05,\ \ 0.06,\ \ 0.07, \\ \frac{T_{\perp c}(0)}{T_{\|c}(0)} &= \frac{\beta_{\perp c}(0)}{\beta_{\|c}(0)} = 1, \\ \frac{T_{\perp h}(0)}{T_{\|h}(0)} &= \frac{\beta_{\perp h}(0)}{\beta_{\|h}(0)} = 9, \\ \beta_{\|c}(0) &= 1, \quad \beta_{\|h}(0) = 1. \end{aligned} \tag{3.6}$$

Physical quantities plotted along the x axis and along the y axis are the same as those in figure 1. Variations in the relative hot proton density, δ, and other fixed parameters are given in the figure title and within the plot. We note an enhancement of the real oscillatory frequency for the higher hot proton population case. Shown in the bottom panel, we note a significant rise in the proton instability growth and instability domain for the initial higher hot proton relative density, i.e. $\delta = 0.07$. Such a notable increase in the real (oscillatory) frequency and growth rate is contributed by the large free energy associated with higher hot proton population in the form of perpendicular temperature anisotropy.

As a result of PC instability, the velocity distributions of cold and hot protons evolve in time t due to diffused pitch angle scattering in velocity space (Seough *et al*. 2014; Kim 2017). Quasilinear theory is one of the effective tools to quantify such a scattering phenomenon in the nonlinear regime of instability development. In response to the PC instability initiated by the hot proton anisotropy, the hot

https://doi.org/10.1017/S0022377825100639 Published online by Cambridge University Press

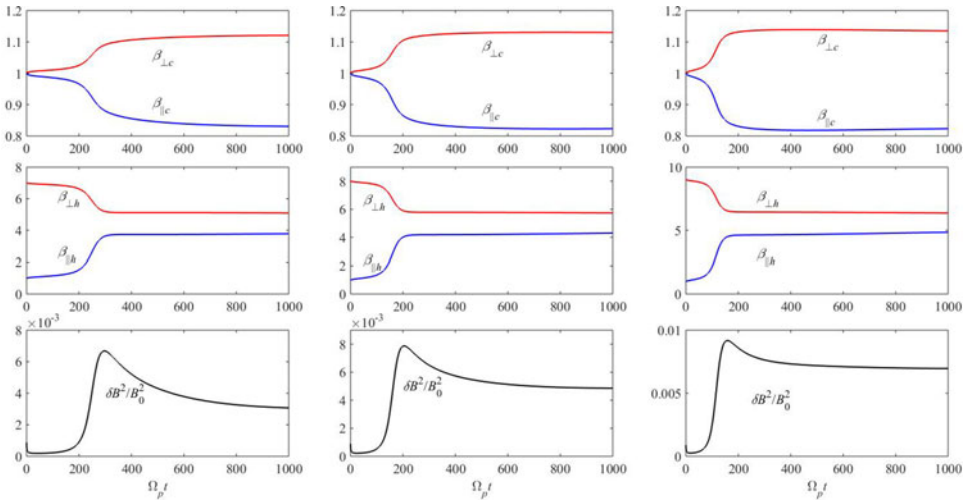

FIGURE 3. The PC instability in the quasilinear regime: effect of hot proton anisotropy on time evolution in temperature (beta) for cold proton component, $\beta_{\perp c}$ and $\beta_{\parallel c}$ (top), hot proton component, $\beta_{\perp h}$ and $\beta_{\parallel h}$ (middle), and wave intensity, $\delta B^2/B_0^2$ (bottom), versus normalised time, $\tau = \Omega_p t$.

proton components cannot maintain the anisotropy level and saturate eventually at a certain lower magnitude. In figure 3 we uncover/quantify the effects of hot proton anisotropy variation on the initial forms of cold/hot proton velocity distributions and associated wave-energy density. To get quantitative predictions, we adopt the following set of initial parameters typical of magnetospheric conditions:

$$\begin{aligned} W(k) &= 5 \times 10^{-4}, \quad \delta = 0.07, \\ \frac{T_{\perp c}(0)}{T_{\parallel c}(0)} &= \frac{\beta_{\perp c}(0)}{\beta_{\parallel c}(0)} = 1, \quad \beta_{\parallel c}(0) = 1, \\ \frac{T_{\perp h}(0)}{T_{\parallel h}(0)} &= \frac{\beta_{\perp h}(0)}{\beta_{\parallel h}(0)} = 7,\ 8,\ 9, \quad \beta_{\parallel h}(0) = 1. \end{aligned} \tag{3.7}$$

In figure 3, the leftmost column adopts the initial parameters of $T_{\perp c}(0)/T_{\parallel c}(0) = 1$, $\beta_{\parallel c}(0) = 1$, and $T_{\perp h}(0)/T_{\parallel h}(0) = 5$, $\beta_{\parallel h}(0) = 1$; the middle column initial values of $T_{\perp c}(0)/T_{\parallel c}(0) = 1$, $\beta_{\parallel c}(0) = 1$, and $T_{\perp h}(0)/T_{\parallel h}(0) = 7$, $\beta_{\parallel h}(0) = 1$; and the rightmost column initial parameters of $T_{\perp c}(0)/T_{\parallel c}(0) = 1$, $\beta_{\parallel c}(0) = 1$, and $T_{\perp h}(0)/T_{\parallel h}(0) = 9$, $\beta_{\parallel h}(0) = 1$. Vertical axis represents the profiles of time-varying core proton plasma betas, $\beta_{\perp c}, \beta_{\parallel c}$, in the top row; hot proton plasma betas, $\beta_{\perp h}, \beta_{\parallel h}$, in the middle row; and associated wave-energy density, $\delta B^2/B_0^2$, in the bottom row. To quantify the time intervals for the saturation of particle distribution and wave intensity, we define a dimensionless quantity $\tau = \Omega_p t$ (time normalised with PC frequency) along the horizontal direction for all cases. Based on the observations of the Earth's outer magnetospheric regions (Gary *et al*. 1994, 1995), we keep the cold proton beta, hot proton beta, cold proton anisotropy and relative density of hot protons as fixed, i.e $\beta_{\parallel c} = 1$, $\beta_{\parallel h} = 1$, $T_{\perp c}/T_{\parallel c} = 1$ and $\delta = 0.05$, respectively, for all our numerically executed output. Shown in the upper panel of the leftmost column, initially isotropic cold protons develop anisotropy, although minimal, through the perpendicular heating (see the gradual rise in $\beta_{\perp c}$) and concomitantly parallel cooling (shown by the

https://doi.org/10.1017/S0022377825100639 Published online by Cambridge University Press

smooth falling of $\beta_{\parallel c}$). In the resonant velocity space, isotropic protons get pitch-angle-scattered through diffusion and end up with some anisotropy in the nonlinear phase of PC instability. Below the cold protons, i.e middle panel of the leftmost column, we note a smooth transit of initially anisotropic hot protons to nearly isotropic state through perpendicular cooling, i.e. fall of $\beta_{\perp h}$, and parallel heating, i.e rise in $\beta_{\parallel h}$ (an opposite effect compared with cold protons). At resonance, hot protons with higher perpendicular velocities get significantly scattered to end up with a nearly Maxwellian form in the interval $\tau = [600-1000]$. In the bottom, we plot wave-energy density to confirm the possible plateau formation of the initial distribution of hot protons. We observe an exponential rise of the wave intensity from its initial noise level which cuts in the interval $\tau = [250-350]$. Afterwards, we also note a reabsorption and regain in the wave intensity until the terminal point of the simulation. Moving on to the middle and rightmost panels, we adopt a relatively higher proton anisotropy ratio, i.e $T_{\perp h}/T_{\parallel h} = 7$ (middle) and $T_{\perp h}/T_{\parallel h} = 9$ (right), keeping other initial parameters fixed. The immediate outcomes of such changes appear in the form of speedy recovery/saturation of hot proton anisotropy, i.e $\tau = [180-210]$ in the middle panels and $\tau = [160-200]$ for the rightmost panels. We also note a quick response of cold protons to attain the anisotropy values on the earlier time scales. Similarly, the associated wave-energy density also displays drastic revisions in response to the new hot proton anisotropy. We display a relatively fast saturation and higher intensity cut levels in the middle and right panels compared with left ones. Such important changes in the particle–wave dynamics (excitation and saturation) are attributed to the availability of more free energy to initiate the PC instability and higher proton scattering through diffusion in velocity space.

Like the real oscillatory frequency and growth rate of the PC mode, hot proton density also affects the relaxation/saturation of the proton distribution and resulting wave-energy density. To quantify the role of varying hot proton population in the wave dynamics, we sketch figure 4 based on the following set of initial conditions:

$$\begin{aligned} W(k) &= 5 \times 10^{-4}, \\ \delta &= 0.05,\ 0.06,\ 0.07, \\ \frac{T_{\perp c}(0)}{T_{\parallel c}(0)} &= \frac{\beta_{\perp c}(0)}{\beta_{\parallel c}(0)} = 1, \quad \beta_{\parallel c}(0) = 1, \\ \frac{T_{\perp h}(0)}{T_{\parallel h}(0)} &= \frac{\beta_{\perp h}(0)}{\beta_{\parallel h}(0)} = 9, \quad \beta_{\parallel h}(0) = 1. \end{aligned} \tag{3.8}$$

In figure 4, the leftmost column is plotted with initial conditions of of $\delta = 0.04$, $T_{\perp c}(0)/T_{\parallel c}(0) = 1$, $\beta_{\parallel c}(0) = 1$, and $T_{\perp h}(0)/T_{\parallel h}(0) = 7$, $\beta_{\parallel h}(0) = 1$; the middle column with initial values of $\delta = 0.06$, $T_{\perp c}(0)/T_{\parallel c}(0) = 1$, $\beta_{\parallel c}(0) = 1$, and $T_{\perp h}(0)/T_{\parallel h}(0) = 7$, $\beta_{\parallel h}(0) = 1$; and the rightmost column with initial parameters of $\delta = 0.08$, $T_{\perp c}(0)/T_{\parallel c}(0) = 1$, $\beta_{\parallel c}(0) = 1$, and $T_{\perp h}(0)/T_{\parallel h}(0) = 7$, $\beta_{\parallel h}(0) = 1$, $\beta_{\parallel h}(0) = 0.6$. Such a combination of input conditions is also typical of magnetospheric plasma conditions. We make a choice of fixed anisotropy ratio and plasma betas of constituent proton components as indicated in (3.7). Labelling and variation of beta profiles largely resemble the results displayed in figure 2. As the PC instability evolves in time t, the initial isotropic cold protons attain a certain anisotropy magnitude following a perpendicular rise (heating) in $\beta_{\perp c}$ and concomitantly fall (or cooling) in $\beta_{\parallel c}$ shown in the leftmost top panel. On the other hand, hot protons displayed in the middle panel (leftmost) tend to relax their initial anisotropy level with a gradual fall in $\beta_{\perp h}$ and rise in the opposite direction, i.e. $\beta_{\parallel h}$. We note a similar time interval of

https://doi.org/10.1017/S0022377825100639 Published online by Cambridge University Press

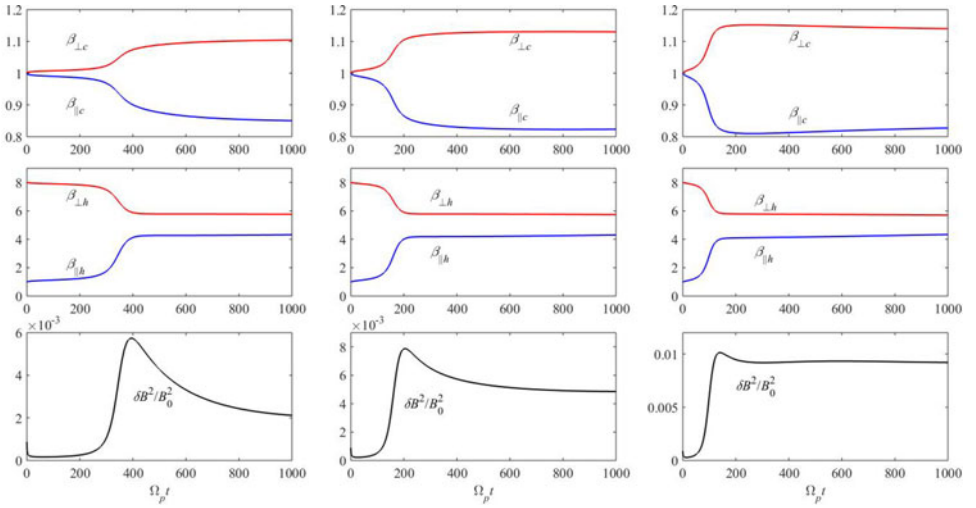

FIGURE 4. The PC instability in the quasilinear regime: effect of hot proton relative density on time evolution in temperature (beta) for cold proton component, $\beta_{\perp c}$ and $\beta_{\parallel c}$ (top), hot proton component, $\beta_{\perp h}$ and $\beta_{\parallel h}$ (middle), and wave intensity, $\delta B^2/B_0^2$ (bottom), versus normalised time, $\tau = \Omega_p t$.

$\tau = [200-300]$ to develop the anisotropy of cold protons and saturation/relaxation of the hot protons. The wave-energy density increases at initial time which eventually saturates following the hot proton relaxation time intervals. For the initial higher hot proton population (results displayed in middle and rightmost panels), we note an appreciable rise in the wave-intensity saturation and speedy recovery of hot protons towards a lower anisotropy ratio. Such an important outcome signifies the greater free energy associated with large anisotropic hot proton density.

The role of PC instability in constraining the high perpendicular temperature is displayed again in figure 5. We replot the findings of figure 3 in the phase space formed by the plasma beta, $\beta_{\parallel}$, and temperature anisotropy, $T_{\perp}/T_{\parallel}$. Guided by the results of Shaaban *et al*. (2016), we have differentiated the stable versus unstable part for the proton states. We show the dynamical trajectories of initial unstable hot protons towards stable regions. Wave-energy density associated with unstable PC instability is depicted with colour code shown in the vertical bar. Evident from the plot, isotropic cold protons attain a certain anisotropy as a result of wave–particle interaction and settle down within the stable part of the plot. Higher anisotropy of hot protons is compensated with excitation of PC instability and a move towards the stable region. They are relocated well below the marginal stability curves with relatively lower anisotropy compared with their initial positions. Through the perpendicular cooling and parallel heating resulting from PC, proton trajectories are significantly influenced in phase space. Notably, the relaxation process for hot protons with high initial anisotropy is relatively rapid, especially at elevated wave-energy densities, which are illustrated in colour coding along the dynamic paths. As shown in figure 5, initially isotropic protons achieve similar temperature anisotropies and occupy comparable states of anisotropy in phase space. In contrast to hot protons, cold protons experience perpendicular heating and cool along the magnetic field during resonant interactions with cyclotron instability. Additionally, the response of cold protons is abrupt, with a large associated energy density indicated in the

https://doi.org/10.1017/S0022377825100639 Published online by Cambridge University Press

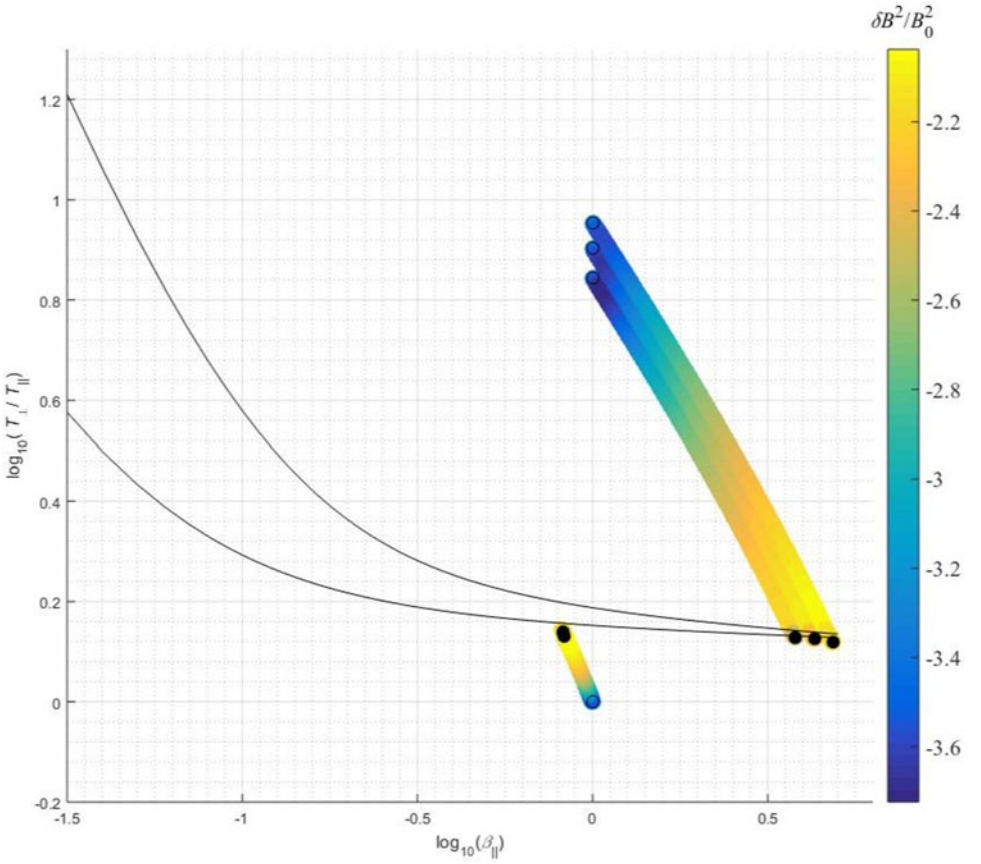

FIGURE 5. Combined particle–wave evolution in response to the PC instability: magnetospheric cold and hot proton trajectories from initial to final positions in the phase space formed by $T_\perp/T_\parallel$ and $\beta_\parallel$. We have colour-coded the resulting wave-energy density as indicated in the sidebar.

right-hand vertical bar. Such an important behaviour of cold/hot protons can also be attributed to the PC instability driven unstable solely by the tenuous hot proton component. Figure 5, therefore, provides a rapid demonstration to unlock the important role of PC instability in defining the perpendicular temperature of hot protons in the magnetospheric regions of space plasmas.

4. Summary and discussion

Various space plasma dynamics, e.g. solar wind and Earth's magnetosphere, are governed/dictated by collective and collisional physical mechanisms. Under certain geometrical and thermal conditions, microinstabilities resulting from the collective processes solely predict and determine charged particle states. Our present study predicts the key role of PC instability in constraining the rapid rise in the perpendicular temperature and defines the threshold values of the unstable PC mode. This instability is left-hand-polarised and operative under high perpendicular temperature, i.e. $T_{\perp p} > T_{\parallel p}$. Such a combination of initial conditions is frequently observed in magnetospheric regions by different space missions and motivates us to find the effective contribution of PC instability. Observations made over the years in magnetospheric

https://doi.org/10.1017/S0022377825100639 Published online by Cambridge University Press

regions (Gary *et al*. 1994, 1995; Toledo *et al*. 2021; Liu *et al*. 2024) suggest adopting multi-component cold and hot proton species. We model the anisotropic hot protons with the bi-Maxwellian form of the velocity distribution. We further assume time variations in the initial isotropic temperature of cold protons and anisotropic temperature of hot protons to study the detailed dynamics of the instability in the quasilinear regime. Different simulation studies appearing in the literature validate and confirm our approximations regarding the initial distribution.

In the present study, we reveal the role of unstable PC instability in dictating the dynamics of outer magnetospheric regions. The choice of initial condition set-up composed of temperature anisotropy and plasma betas are typical of the Earth's outer magnetosphere. We note an appreciable rise in the growth rate and the domain of the instability for large initial hot proton anisotropy and population. Quasilinear evolution of PC instability helps us to understand and quantify the wave-energy saturation and relaxation of hot proton temperatures. Higher temperature anisotropy and the number density of hot protons largely favour the relaxation/saturation mechanism and wave-energy density cutoffs. Such conclusions are attributed to the availability of more free energy (high temperature anisotropy and population of hot protons) to pump the instability and abruptly leads to isotropisation/relaxation. Dynamical paths in phase space show the final destinations of both core versus halo proton components near or below the marginal stability curves.

Our present analysis is limited to establishing a theoretical framework for the PC instability and its time evolution in the Earth's outer magnetospheric environments. To validate such comprehensive results based on a mathematical model, a comparison against a more rigorous particle-in-cell simulation is called for. In some recent developments, side-by-side comparisons against simulation and observations are reported for the combined wave spectrum of electron-cyclotron mirror (Sarfraz *et al*. 2022) and PC mirror (Yoon *et al*. 2022). Observations are particularly attained via WIND spacecraft SWE Faraday cup observations (Ogilvie *et al*. 1995). For the other regions where observations suggest the presence of suprathermal charged particles, our present formalism can principally be extended to incorporate the non-thermal effects (Shaaban *et al*. 2021) and radial expansion effects too (Yoon & Sarfraz 2017). One of the key perspectives is to extend such a scheme for oblique propagation and see its impact on the instability thresholds and possibly evolution in the quasilinear regime.

Acknowledgements

Editor Thierry Passot thanks the referees for their advice in evaluating this article.

Data availability statement

The data that support the findings of this study are available from the corresponding author upon reasonable request.

Declaration of interests

The authors report no conflict of interest.

REFERENCES

Anderson, B.J., Denton, R.E., Ho, G., Hamilton, D.C., Fuselier, S.A. & Strangeway, R.J. 1996 Observational test of local proton cyclotron instability in the Earth's magnetosphere. *J. Geophys. Res.* **101**, 21527–21543.

BILAL, M., UR REHMAN, A., AHMAD, M., SHAHZAD, M.A., SARFRAZ, M. & MAHMOOD, S. 2023 Linear analysis of whistler mode instability in anisotropic q-nonextensive distributed plasmas. *Phys. Scr*. **98**, 095607.

CHEW, GF., GOLDBERGER, ML. & LOW, F.E. 1956 The Boltzmann equation an d the one-fluid hydromagnetic equations in the absence of particle collisions. *Proc. R. Soc. Lond. A*. **236**, 112–118.

FELDMAN, W.C., ASBRIDGE, J.R., BAME, S.J., MONTGOMERY, M.D. & GARY, S.P. 1975 Solar wind electrons. *J. Geophys. Res.* **80**, 4181–4196.

GARY, S.P. & FELDMAN, W.C. 1977 Solar wind heat flux regulation by the Whistler instability. *J. Geophys. Res.* **82**, 1087–1094.

GARY, S.P., FELDMAN, W.C., FORSLUND, D.W. & MONTGOMERY, M.D. 1975 Electron heat flux instabilities in the solar wind. *Geophys. Res. Lett.* **2**, 79–82.

GARY, S.P. & WINSKE, D. 1990 Computer simulations of electromagnetic instabilities in the plasma sheet boundary layer. *J. Geophys. Res.* **95**, 8085–8094.

GARY, S.P., MOLDWIN, M.B., THOMSEN, M.F., WINSKE, D. & MCCOMAS, D.J. 1994 The whistler heat flux instability: threshold conditions in the solar wind. *J. Geophys. Res.* **99**, 23603.

GARY, S.P., THOMSEN, M.F., YIN, L. & WINSKE, D. 1995 Electromagnetic proton cyclotron instability: interactions with magnetospheric protons. *J. Geophys. Res.* **100**, 21961.

GARY, S.P. 1992 The mirror and ion cyclotron anisotropy instabilities. *J. Geophys. Res.* **97**, 8519–8529.

GARY, S.P. 1993 *Theory of Space Plasma Microinstabilities*. Cambridge University Press.

HARRIS, E.G. 1961 J Plasma instabilities associated with anisotropic velocity distributions. *Nucl. Energy, Part C, Plasma Phys.* **2**, 138–145.

HELLINGER, P., TRÁVNÍČEK, P.M., DECYK, V.K. & SCHRIVER, D. 2014 Oblique electron fire hose instability: Particle-in-cell simulations. *J. Geophys. Res.: Space Phys.* **119**, 59–68.

ISENBERG, P.A., MARUCA, B.A. & KASPER, J.C. 2013 Self-consistent ion cyclotron anisotropy-beta relation for solar wind protons. *ApJ* **773**, 164.

KIM, H.P., HWANG, J., SEOUGH, J.J. & YOON, P.H. 2017 Electron temperature anisotropy regulation by whistler instability. *J. Geophys. Res.: Space Phys.* **122**, 4410–4419.

LAZAR, M., POEDTS, S., SCHLICKEISER, R. & DUMITRACHE, C. 2015 Towards realistic parametrization of the kinetic anisotropy and the resulting instabilities in space plasmas. Electromagnetic electron-cyclotron instability in the solar wind. *Mon. Not. R. Astron. Soc.* **446**, 3022–3033.

LAZAR, M., YOON, P.H., LÓPEZ, R.A. & MOYA, P.S. 2018 Electromagnetic electron cyclotron instability in thesolar wind. *J. Geophys. Res.: Space Phys.* **123**, 6–19.

LEE, S-Y., LEE, E., SEOUGH, J., LEE, J-GI, HWANG, J., LEE, J-J., CHO, K-S. & YOON, P.H. 2018 Simulation and quasi-linear theory of whistler anisotropy instability. *J. Geophys. Res.* **123**, 3277–3290.

LIU, X. *et al.* 2024 Simultaneous observations of mirror mode structures and electromagnetic ion cyclotron waves in the earth's outer magnetosphere. *J. Geophys. Res.: Space Phys.* **129**, e2024JA032951.

MAKSIMOVIC, M., *et al.* 2005 Radial evolution of the electron distribution functions in the fast solar wind between 0.3 and 1.5 AU. *J. Geophys. Res.* **3110**, A09104.

MARUCA, B.A., KASPER, J.C. & GARY, S.P. 2012 Instability-driven limits on helium temperature anisotropy in the solar wind: observations and linear Vlasov analysis. *ApJ* **748**, 137.

MATTEINI, L., HELLINGER, P., LANDI, S., TRÁVNÍČEK, P.M. & VELLI, M. 2012 Ion kinetics in the solar wind: coupling global expansion to local microphysics. *SSRv* **172**, 373.

OGILVIE, K.W., *et al.* 1995 SWE, a comprehensive plasma instrument for the WIND spacecraft. *Space Sci. Rev.*. **71**, 55–77.

SAGDEEV, R.Z. & SHAFRANOV, V.D. 1961 Plasma instabilities associated with anisotropic velocity distributions. *JETP* **12**, 130.

SARFRAZ, M. & YOON, P.H. 2019 Contributions of protons in electron firehose instability driven by solar wind core–halo electrons. *Mon. Not. R. Astron. Soc.* **486**, 3550–3559.

SARFRAZ, M., SAEED, S., YOON, P.H., ABBAS, G. & SHAH, H.A. 2016 Macroscopic quasilinear theory of electromagnetic electron cyclotron instability associated with core and halo solar wind electrons. *J. Geophys. Res.* **121**, 9356–9368.

https://doi.org/10.1017/S0022377825100639 Published online by Cambridge University Press

SARFRAZ, M., SAEED, S., YOON, P.H., ABBAS, G. & SHAH, H.A. 2017 Macroscopic quasilinear theory of parallel electron firehose instability associated with solar wind electrons. *Phys. Plasmas*. **24**, 012907.

SARFRAZ, M. 2018 A moment-based quasilinear theory for electron firehose instability driven by solar wind core/Halo electrons. *J. Geophys. Res.* **123**, 6107–6118.

SARFRAZ, M., LÓPEZ, R.A., AHMED, S. & YOON, P.H. 2022 Electron mirror and cyclotron instabilities for solar wind plasma. *MNRAS* **509**, 3764.

SCHLICKEISER, R. 2002 *Cosmic Ray Astrophysics*. Springer.

SEOUGH, J. & YOON, P.H. 2012 Quasilinear theory of anisotropy-beta relations for proton cyclotron and parallel firehose instabilities. *J. Geophys. Res.* **117**, A08101.

SEOUGH, J., YOON, P.H., KIM, K.-H. & LEE, D.-H. 2013 Solar wind proton anisotropy versus beta relation. *Phys. Rev. Lett.* **110**, 071103.

SEOUGH, J., YOON, P.H. & CHWANG, P.H. 2014 Quasilinear theory and particle-in-cell simulation of proton cyclotron instability. *Phys. Plasmas*. **21**, 062118.

SEOUGH, J., YOON, P.H., HWANG, J. & NARIYUKI, Y. 2015 Simulation and quasilinear theory of aperiodic ordinary mode instability. *Phys. Plasmas*. **22**, 082122.

SHAABAN, S.M., LAZAR, M., POEDTS, S. & ELHANBALY, A. 2016 The interplay of the solar wind proton core and halo populations: EMIC instability. *J. Geophys. Res.: Space Phys.* **121**, 6031–6047.

SHAABAN, S.M., LAZAR, M., YOON, P.H. & POEDTS, S. 2019 The interplay of the solar wind core and suprathermal electrons: a quasilinear approach for firehose instability. *ApJ* **871**, 237.

SHAABAN, S.M., LAZAR, M. & SCHLICKEISER, R. 2021 Electromagnetic ion cyclotron instability stimulated by the suprathermal ions in space plasmas: a quasi-linear approach. *Phys. Plasmas*. **28**, 022103.

STVERAK, S., TRAVNICEK, P., MAKSIMOVIC, M., MARSCH, E., FAZAKERLEY, A.N. & SCIME, E.E. 2008 Electron temperature anisotropy constraints in the solar wind. *J. Geophys. Res.* **113**, A03103.

TOLEDO-REDONDO, S. *et al.* 2021 Kinetic interaction of cold and hot protons with an oblique EMIC wave near the dayside reconnecting magnetopause. *Geophys. Res. Lett.* **48**, e2021GL092376.

VINAS, A., GURGIOLO, C., NIEVES-CHINCHILLA, T., GARRY, S.P. & GOLSTEINA, M.L. 2010 Whistler waves driven by anisotropic strahl velocity distributions: cluster observations. *AIP Conf. Proc.* **1216**, 265–270.

YOON, P.H. & SARFRAZ, M. 2017 Interplay of electron and proton instabilities in expanding solar wind. *Astrophys. J.* **835**, 246.

YOON, P.H. & SEOUGH, J. 2012 Quasilinear theory of anisotropy-beta relation for combined mirror and proton cyclotron instabilities. *J. Geophys. Res.* **117**, A08102.

YOON, P.H., SEOUGH, J., KIM, K.H. & LEE, D.H. 2012 Empirical versus exact numerical quasilinear analysis of electromagnetic instabilities driven by temperature anisotropy. *J. Plasma Phys.* **78**, 47–54.

YOON, P.H., LÓPEZ, R.A., SEOUGH, J. & SARFRAZ, M. 2017 Velocity moment-based quasilinear theory and particle-in-cell simulation of parallel electron firehose instability. *Phys. Plasmas*. **24**, 112104.

YOON, P.H., SEOUGH, J., HWANG, J. & NARIYUKI, Y. 2015 Macroscopic quasi-linear theory and particle-in-cell simulation of helium ion anisotropy instabilities. *J. Geophys. Res.: Space Phys.* **120**, 6071–6084.

YOON, P.H., SARFRAZ, M., ALI, Z., SALEM, C.S. & SEOUGH, J. 2022 Proton cyclotron and mirror instabilities in marginally stable solar wind plasma. *MNRAS* **509**, 4736.

YOON, P.H., SALEM, C.S., KLEIN, K.G., MARTINOVIĆ, M.M., LÓPEZ, R.A., SEOUGH, J., SARFRAZ, M., LAZAR, M. & SHAABAN, S.M. 2024 Regulation of solar wind electron temperature anisotropy by collisions and instabilities. *ApJ* **975**, 105.

https://doi.org/10.1017/S0022377825100639 Published online by Cambridge University Press